

Hydrodynamic flow at RHIC

Peter F. Kolb^{1,2,a}

¹ Institut für Theoretische Physik
Universität Regensburg
D-93040 Regensburg, Germany

² Department of Physics
The Ohio State University
174 West 18th Avenue
Columbus, OH 43210, USA

^a E-mail: pkolb@mps.ohio-state.edu

Abstract. We review the apparently hydrodynamic behaviour of low transverse momentum particles ($p_T \leq 1.5$ GeV/ c) produced in central and semicentral ($b \leq 7$ fm) heavy ion collisions at RHIC. We investigate the impact parameter dependence of various observables, elaborating on radial and elliptic flow and particle multiplicities. We also discuss possible ambiguities in the initialization of the hydrodynamic system and present observables that should allow for their resolution.

Keywords: Relativistic heavy-ion collisions, flow, hydrodynamic model
PACS: 25.75-q, 25.75.Ld

1. Introduction and Motivation

The first measurements at RHIC that systematically investigated the centrality dependence of an observable focused on elliptic flow (the anisotropic particle emission from the collision) [1], followed by the centrality dependence of the absolute (charged) particle yield per unit of pseudorapidity [2] and the produced transverse energy per unit of pseudorapidity [3]. Such systematic studies of the influence of the collision centrality are of fundamental interest, as they represent a powerful tool to gain a detailed understanding of the collision dynamics:

Firstly, non-central collisions offer additional observables due to their deformed, almond shaped overlap region, which can lead to angular dependencies (relative to the reaction plane) of final state observables which do not appear in central collisions with azimuthal symmetry [4]. Large anisotropies arise only if there is strong rescattering already

in the first moments ($\sim \text{fm}/c$) of the collision, and (anisotropic) pressure gradients are building up, determining the subsequent evolution of the matter. Curiously the stronger forces in the direction of steepest pressure gradients lead to more transport of matter in those directions and thus eventually even out the differences between the radial gradients in the short and long direction of the initial almond. Thus anisotropies that are observable in the final state are built up early and in the hottest stages of the collision, as the cause of these anisotropies disappears during the system's evolution (on a timescale of less than $\sim 4 \text{ fm}/c$ [5, 6, 7]). In contrast to this self-quenching effect e.g. for elliptic flow, other dynamical quantities such as radial flow continue to grow until freeze-out and carry information about the full expansion stage. We explore the influence of the initial spatial anisotropies in terms of a hydrodynamic picture, which represents the limiting case of maximum response to the initially produced pressure gradients due to strong (infinite) rescattering already in the early stages of the expansion. Such an approach was shown to be appropriate at RHIC energies [8] and is valuable to understand the global (macroscopic) characteristics of the expansion stage of an ultrarelativistic heavy ion collision.

Secondly, changing the centrality leads to a varying number of participating nucleons and a changing size of the interaction region. The amount of energy deposited in the collision region as well as the energy density in the system will be largest in central collisions and decrease with increasing impact parameter. Thus by varying the centrality, one is able to scan the initial energy density and in this fashion can measure excitation functions even without varying the beam energy. It is crucial however to disentangle such 'centrality excitation functions' from the geometric effects introduced by the varying eccentricity of the system. In this spirit we investigate the centrality dependence of particle production per participating nucleon pair and transverse energy carried by the emitted hadrons to learn about soft and hard scattering contributions in the initial processes.

In section 2, we introduce the underlying assumptions of hydrodynamic models and focus especially on different initialization scenarios. We present our results and comparisons to experimental data in Section 3, which covers a discussion of particle spectra and radial flow, elliptic flow, multiplicities and transverse energy. Section 4 contains a brief summary. In the Appendix we study the effect of boost invariance on the pseudorapidity dependence of multiplicities and elliptic flow. This helps to understand the corresponding shapes of the recently presented experimental data [9] around midrapidity.

2. Hydrodynamics and Initialization

Hydrodynamics is a macroscopic approach to describe the dynamical evolution of the expansion stage of a heavy ion collision. It is a phenomenological model that, by describing the evolution of thermodynamic fields like energy density, pressure, temperature and flow fields, circumvents the necessity of introducing unknown microscopic parameters (e.g. in-medium cross sections or string tensions) as required for microscopic descriptions of such systems.

In the hydrodynamic description the nuclear equation of state enters the model quite naturally as the connection of pressure or temperature to energy and particle density. How-

ever it is not at all obvious that such an approach is feasible at all, as a thermodynamic treatment requires a 'large', 'macroscopic' system in local thermal equilibrium and an adiabatic expansion stage. But the good agreement of hydrodynamic simulations and experimental data from RHIC in fact point towards such rapid thermalization followed by a hydrodynamic expansion.

The effective treatment however lacks a physical understanding of the underlying microscopic processes and the early equilibration time as well as an explanation of the obviously very large rescattering rates. It must then eventually be supplemented by a microscopic kinetic treatment to check its validity. Finally a hydrodynamic approach is only valid for a certain timespan of the expansion. We therefore have to introduce assumptions about initialization and freeze-out conditions [8, 11].

Existing microscopic models on the other hand so far lack rescattering mechanisms which are strong enough to explain the large observed anisotropies (see e.g. [12]), or the need to assume unrealistically large cross-sections [13]. Only when coupled to a hydrodynamic initial stage that is able to generate sufficient flow anisotropies before the system enters the hadronic rescattering phase, the large observed anisotropies can be recovered [14]. Recently however progress in purely microscopic models was reported by introducing multi-Pomeron exchanges in quark gluon string models [15].

2.1. Relativistic hydrodynamics and equation of state

Adiabatic expansion of matter is described by the hydrodynamic equations for the conservation of energy, momentum and baryon number. In relativistic form they read

$$\partial_\mu T^{\mu\nu} = 0, \quad \partial_\mu j^\mu = 0, \quad (1)$$

with the energy-momentum tensor and the baryon current

$$T^{\mu\nu}(x) = (e(x) + p(x))u^\mu(x)u^\nu(x) - g^{\mu\nu}p(x), \quad j^\mu(x) = n(x)u^\mu(x). \quad (2)$$

These equations for the space-time evolution of the physical fields are closed by an equation of state (EoS) relating energy and baryon density to the pressure and temperature. The EoS for this study contains a sharp first order phase transition, which connects a hadronic resonance gas at low energy densities ($e < 0.45 \text{ GeV/fm}^3$) to the hard equation of state of an ideal ultrarelativistic gas (modeling a quark gluon plasma phase) in the high energy density region of the phase space diagram ($e > 1.6 \text{ GeV/fm}^3$). Further details on the equation of state and its construction can be found in [7], which also includes a discussion of the influence of the phase transition and details of the equation of state on final state observables.

To reduce computational costs we analytically implement boost-invariance in longitudinal direction. The shape of the measured $dN/d\eta$ distribution [10] indicates that this is well satisfied around midrapidity at RHIC energies (see Appendix). Fully three-dimensional calculations exist for SPS energies [16] and are under development for RHIC energies.

2.2. Initialization

The linear scaling of particle production with the number of wounded nucleons as observed at SPS energies [17] indicates that the first scattering processes underlying such collisions are soft or non-perturbative, and that it is the number of wounded nucleons that governs particle production. We assume this to hold locally in the transverse plane and the number of produced particles to be proportional to the number of participants per unit area. For a collision with impact parameter \mathbf{b} this density at a point \mathbf{s} in the transverse plane is given by

$$n_{\text{WN}}(\mathbf{s}; \mathbf{b}) = T_A(\mathbf{s} + \frac{1}{2}\mathbf{b}) \left[1 - \left(1 - \frac{\sigma T_B(\mathbf{s} - \frac{1}{2}\mathbf{b})}{B} \right)^B \right] + T_B(\mathbf{s} - \frac{1}{2}\mathbf{b}) \left[1 - \left(1 - \frac{\sigma T_A(\mathbf{s} + \frac{1}{2}\mathbf{b})}{A} \right)^A \right],$$

where we have introduced the nuclear thickness function

$$T_A(\mathbf{s}) = \int_{-\infty}^{+\infty} dz \rho_A(\mathbf{s}, z),$$

with $\rho_A(\mathbf{s}, z)$ parametrizing the nuclear density profile (i.e. a Woods Saxon profile with appropriate parameters for a nucleus with mass number A).

On the other hand one expects the particle production from hard collisions to dominate at high energies. This perturbative particle production scales with the number of collisions, which is given per unit area in the transverse plane by

$$n_{\text{BC}}(\mathbf{s}; \mathbf{b}) = \sigma T_A(\mathbf{s} + \frac{1}{2}\mathbf{b}) T_B(\mathbf{s} - \frac{1}{2}\mathbf{b}).$$

In the following we study the results obtained using five different parametrizations of the initial state. We assume either energy or entropy density to be proportional to n_{WN} (parametrizations labeled eWN and sWN, respectively) or to n_{BC} (labeled eBC and sBC, respectively). In addition we use an initialization resulting from a saturation model calculation which limits the growth of the gluonic cross-section in the transverse plane on the basis of geometrical arguments [18], and label these results by 'sat'. More details on the initialization models can be found in [11, 18].

3. Experimental Observables

The initialization fields for energy and baryon number density are obtained by a straightforward extrapolation from earlier simulations where we tuned them to fit particle spectra resulting from the most central Pb+Pb collisions at the highest available SPS beam energies [19]. For RHIC energies, we readjust only one parameter (the initial energy density at the origin in $b = 0$ collisions) to reproduce the final particle multiplicity observed in central collisions at RHIC [20]. (The equilibration time is scaled down so that its product with the maximum temperature is the same for RHIC and SPS systems). In our hydrodynamic simulations, this results in a maximum energy density $e_0 = 23 \text{ GeV}/\text{fm}^3$ at an equilibration time $\tau_0 = 0.6 \text{ fm}/c$ (compared to $9 \text{ GeV}/\text{fm}^3$ at $0.8 \text{ fm}/c$ for the earlier SPS simulations). The new initialization leads to a mean energy density of $e_{\text{mean}} = 4.8 \text{ GeV}/\text{fm}^3$ at $\tau = 1.0 \text{ fm}/c$, for which the PHENIX collaboration estimates approximately $5.0 \text{ GeV}/\text{fm}^3$ [3].

3.1. Spectra and radial flow

The larger energy densities and pressure gradients in calculations for RHIC lead to stronger transverse expansion, which is reflected in flatter transverse mass spectra compared to SPS results (Fig. 1 in [21]). This is in good quantitative agreement with preliminary spectra from the RHIC experiments [10]. In the hydrodynamic simulations, the average radial flow velocity at freeze-out increases from $0.45 c$ at maximum SPS-energies to $0.55 c$ at $\sqrt{s_{NN}} = 130$ GeV. The influence of the initialization on the slopes of the particle spectra is weak, but one observes that the spectra are getting flatter in the order eWN, sWN, eBC, sBC with the results for the saturation model somewhere in between sWN and eBC. This reflects the harder initializations of the binary collision models, which results in steeper initial pressure gradients and larger driving forces.

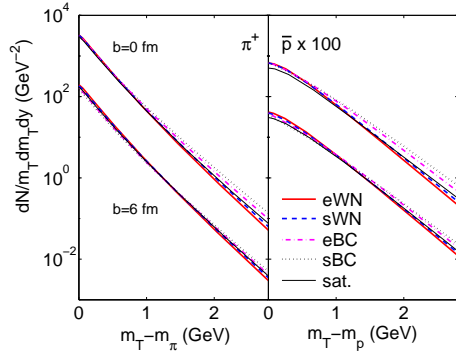


Fig. 1. Transverse mass spectra of pions and antiprotons for central and semicentral collisions (the latter scaled by a factor 0.1) as resulting from the different initializations.

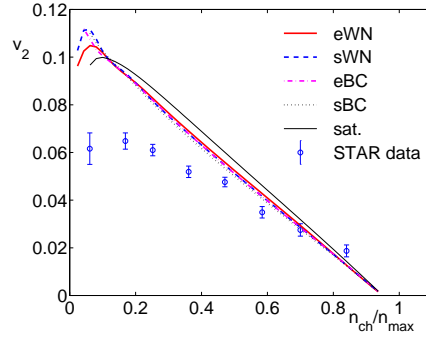


Fig. 2. Elliptic flow of charged hadrons as function of centrality, given by the number of produced particles for the different initializations together with experimental data [1].

3.2. Elliptic flow

The quantitative agreement of hydrodynamic simulations with the measured data for elliptic flow, both for the momentum integrated and the minimum bias averaged differential elliptic flow (for not too large impact parameters and transverse momenta), was pointed out and discussed in an earlier work [8] and is reproduced in Figs. 2 and 3. Here we investigate the influence of the different initialization scenarios.

Fig. 2 shows the momentum integrated elliptic flow as a function of centrality, characterized by the particle yield at midrapidity. There is good agreement with the experimental data for central to semicentral collisions (high to intermediate values of n_{ch}/n_{max}) independently of the underlying initialization (except of the saturated initialization, giving larger

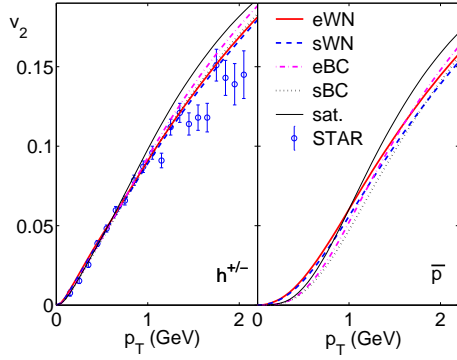


Fig. 3. Elliptic flow in minimum bias configuration for charged hadrons together with the experimental data (left) and antiprotons (right).

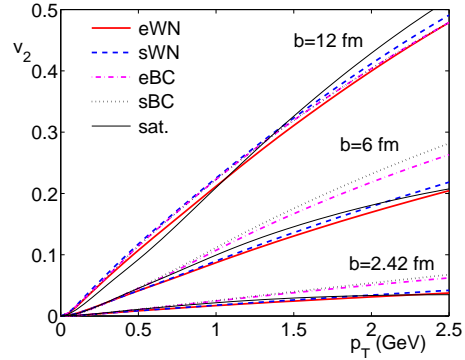


Fig. 4. Elliptic flow of charged hadrons as function of transverse momentum for fixed impact parameters.

anisotropies than the others). Also Fig. 3, which shows minimum bias averaged differential elliptic flow $v_2(p_T)$, reveals that the results for charged hadrons are rather independent of the underlying initialization. Deviations can only be seen at intermediate to high p_T , and then again especially for the saturation model. The analysis of charged hadrons is dominated by pions due to their large abundancies. Analyzing heavier particles independently, as e.g. done for antiprotons in the right panel of Fig. 3, shows that elliptic flow of heavier particles is sensitive on the details of the initialization. Fig. 4 shows differential elliptic flow for specific impact parameters, without averaging over them to yield minimum bias results. Also here a sensitivity on the initialization is seen, especially for semicentral collisions. This sensitivity is lost when averaging over impact parameters which goes ahead with weighting over the resulting particles, as seen in Fig. 3. The centrality dependence of particle production in the different models is thus crucial and therefore studied in the next subsection.

It is truly astonishing that the experimental data and the hydrodynamic results coincide up to impact parameters of about 7 fm and p_T of about 2 GeV. Out of all models applied to relativistic heavy ion collisions, hydrodynamics exhibits the strongest (namely infinite) rescattering, and thus leads to the strongest mapping of initial coordinate anisotropies to final momentum space anisotropies. Hydrodynamics thus gives the upper limit of possible v_2 . That the data reach up to this limit is remarkable!

3.3. Multiplicities and transverse energy

Contrary to the minimum bias elliptic flow analysis, the centrality dependence of particle production is quite sensitive on the details of initialization. The left plot in Fig. 3.3 shows

the number of produced charged hadrons per participating nucleon pair as a function of participants from our simulations together with experimental results [2, 10, 20]. The

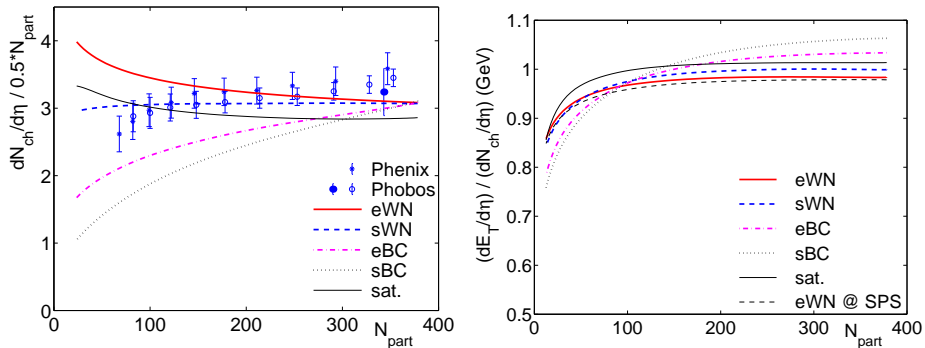


Fig. 5. Charged particle yield per participating nucleon pair (left) and transverse energy per produced particle (right) as functions of participating nucleons.

experimental data disfavor the soft initialization 'eWN' and the saturation model. The other initializations show a tendency similar to the data, i.e. rising particle production for more central collisions. The data would be best described by a combination [23] of the two extremes for hard and soft scattering contributions to particle production that we have studied here. This is under current study within our hydrodynamic approach.

The results for the transverse energy per produced particle are shown in the righthand side plot of Fig. 3.3. Data from the SPS [17] shows qualitative agreement with the shape of the curve from hydrodynamics initialized by a wounded nucleon Ansatz – a saturating transverse energy per particle with a wide plateau from semicentral to central collisions. However very recent experimental data at RHIC [3] show the same shape, disfavoring the hard initializations of our model, which do not follow this trend. A definite statement on that seemingly contradictory behaviour of the centrality dependence of particle production and transverse energy carried per particle has to await a more careful theoretical analysis which is under way.

4. Conclusions

We have reviewed the experimental and theoretical evidence for early equilibration and subsequent hydrodynamic evolution of matter created in heavy ion collisions at RHIC. The large radial and anisotropic flow is most easily explained under the assumption of strong pressure gradients driving the system's expansion. The energy densities at the equilibration timescale reach far beyond the critical energy density. Microscopic simulations with standard scattering cross sections fail to describe flow observables due to a lack of sufficiently

large rescattering.

We further investigated a possible influence of the initialization on the observables. We found that no ambiguity arises for the analysis of the published results on centrality dependence of momentum integrated elliptic flow and transverse momentum dependence of elliptic flow in minimum bias configurations. On the other hand, we discussed observables which would allow for a distinction of the initialization, that is minimum bias elliptic flow for heavier particles (e.g. antiprotons), momentum dependence of elliptic flow for fixed intermediate impact parameters and the transverse energy per produced particle.

Appendix

We briefly discuss the influence of the rapidity (y) \leftrightarrow pseudorapidity (η) transformation on the pseudorapidity dependence of particle yield and elliptic flow under assumption of boost-invariance along the beam axis. This will lead to a quantitative understanding of the experimental data recently presented by the PHOBOS collaboration [9].

We start out with the definitions for the rapidity $y := \text{Atanh}(p_z/E)$ and the pseudorapidity $\eta := \text{Atanh}(p_z/p)$. From these definitions follows the connection of the differentials $dy = \frac{p}{E} \cdot d\eta$ which is the focus of interest.

For this instructive (quantitative) excursion we make very simple model assumptions. We strictly assume boost invariance not only around midrapidity, but assume that all quantities are independent of y , no matter how large y is. For the spectra we use the simple exponentials

$$\frac{dN}{p_T dp_T dy}(p_T) = N e^{-\sqrt{m^2 + p_T^2}/T}$$

where we use for these case studies simply $T = 190$ MeV and $m = m_\pi = 140$ MeV.

Boost invariant, i.e. y independent spectra transform due to the Jacobian to η dependent spectra according to

$$\frac{dN}{p_T dp_T d\eta}(p_T, \eta) = \frac{p_T \cosh \eta}{\sqrt{m^2 + p_T^2 \cosh^2 \eta}} \frac{dN}{p_T dp_T dy}(p_T).$$

This distribution gives thus smaller values than the original one. The suppression is largest for low p_T and vanishes for high p_T . Also the reduction is larger the larger the mass is, and the smaller η (i.e. around midrapidity). For large η the distribution approach each other.

From this it is obvious that the p_T integrated spectra lead to smaller values of $dN/d\eta$ around midrapidity than far away, where it approaches the constant value of dN/dy (left panel of Fig. 6). In reality boost invariance must break down at some rapidity, and the particle yield drops to zero. However the dip observed in the $dN/d\eta$ distribution around midrapidity is thus well expected from a boost-invariant source, and we find in fact quantitative agreement with the preliminary STAR-data [10] from $\eta = -0.5$ to 0.5 .

Rapidity dependent elliptic flow is defined as $v_2(p_T, b, y) = \langle \cos(2\phi) \rangle$ and the same for $v_2(p_T, b, \eta)$ where the averages are taken with respect to the dy respectively $d\eta$ distributions with a fixed impact parameter b . From the definitions one finds easily that

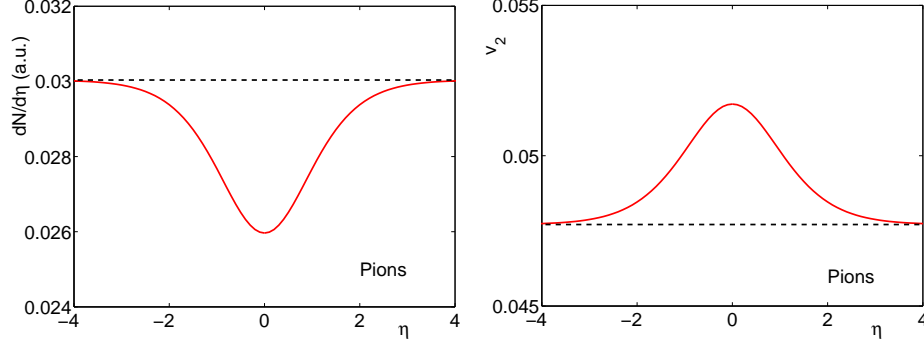


Fig. 6. Transformation of boost-invariant quantities (independent of rapidity y) to pseudorapidity. The left plot shows the effect of the Jacobian of the transformation on the particle spectra, the right plot the influence on the elliptic flow coefficient v_2 .

$v_2(p_T, b, \eta) = v_2(p_T, b, y) = v_2(p_T, b, y = 0)$ and therefore also $v_2(p_T, b, \eta)$ is independent of the pseudorapidity. However for the total elliptic flow, when integrating over the transverse momentum, the pseudorapidity dependence will come into play, due to the different shapes of the spectra:

$$v_2(\eta) = \frac{\int dp_T p_T v_2(p_T) \frac{dN}{p_T dp_T d\eta}(\eta)}{\int dp_T p_T \frac{dN}{p_T dp_T d\eta}(\eta)}.$$

Consider the effect of this: $v_2(p_T)$ is a monotonically increasing function. For large η the weighting particle distributions will become identical to the spectra $dN/p_T dp_T dy$ and therefore we will recover v_2 as weighted with the boost-invariant rapidity-distributions. Now going to smaller pseudorapidities we are weighting the differential elliptic flow with the suppression of the low p_T part. Thus higher p_T 's with larger $v_2(p_T)$ will get stressed and we will have larger p_T -integrated elliptic flow around mid(pseudo)rapidity, than away from it! We illustrate this in Fig. 6, where we used for simplicity the linear relation $v_2(p_T, \eta) = p_T(\text{GeV})/8.5$ which is a first approximation for the experimental results on 'minimum bias' collisions.

Thus, a boost invariant source would show a bump in $v_2(\eta)$ and a dip in the rapidity distribution $dN/d\eta$. In reality we also expect that elliptic flow drops to zero far away from mid-rapidity as in these regions the reaction dynamics does not allow for sufficient equilibration, the primary cause of elliptic flow in non-central collisions.

Acknowledgements

I would like to thank the organizers for the stimulating workshop and especially acknowledge interesting and motivating discussions with J. Aichelin, B. Back, C. Bertulani, R. Lacey, P. Seyboth, and G. Verde.

I have reported on work done in collaboration with K. Eskola, U. Heinz, P. Huovinen and K. Tuominen. P. Huovinen and U. Heinz are thanked for help with the manuscript. This work was supported in parts by the Deutsche Forschungsgemeinschaft.

References

1. K.H. Ackermann *et al.* (STAR Collaboration), Phys. Rev. Lett. **86** (2001) 402.
2. K. Adcox *et al.* (PHENIX Collaboration), Phys. Rev. Lett. **86** (2001) 3500.
3. K. Adcox *et al.* (PHENIX Collaboration), nucl-ex/ 0104015.
4. J.-Y. Ollitrault, Phys. Rev. D **46** (1992) 229.
5. H. Sorge, Phys. Rev. Lett. **78** (1997) 2309; *ibid.* **82** (1999) 2048.
6. B. Zhang, M. Gyulassy, and C.M. Ko, Phys. Lett. B **455** (1999) 45.
7. P.F. Kolb, J. Sollfrank, and U. Heinz, Phys. Rev. C **62** (2000) 054909.
8. P.F. Kolb, P. Huovinen, U. Heinz, and H. Heiselberg, Phys. Lett. B **500** (2001) 232; P. Huovinen, P.F. Kolb, U. Heinz, nucl-th/ 0104020
9. Presentation by the PHOBOS collaboration in [10]; B.B. Back for the PHOBOS collaboration, these proceedings.
10. Proceedings of “Quark Matter 2001” (Stony Brook, Jan. 15-20, 2001), to appear in Nucl. Phys. A. Transparencies of the contributions are available at <http://www.rhic.bnl.gov/qm2001/program.html>.
11. P.F. Kolb, U. Heinz, P. Huovinen, K.J. Eskola, and K. Tuominen, hep-ph/ 0103234
12. M. Bleicher, and H. Stöcker, hep-ph/ 0006147.
13. D. Molnár, and M. Gyulassy, nucl-th/ 0104018.
14. D. Teaney, J. Lauret, and E.V. Shuryak, nucl-th/ 0011058, nucl-th/ 0104041.
15. E.E. Zabrodin, C. Fuchs, L.V. Bravina, and A. Faessler, nucl-th/ 0104054.
16. T. Hirano, Phys. Rev. Lett. **86** (2001) 2754; C. Nonaka, E. Honda, and S. Muroya, Eur. Phys. J. C **17** (2000) 663
17. M.M. Aggarwal *et al.* (WA98 Collaboration), Eur. Phys. J. C **18** (2001) 651.
18. K.J. Eskola, K. Kajantie, P.V. Ruuskanen, and K. Tuominen, Nucl. Phys. **B570** (2000) 379; K.J. Eskola, K. Kajantie, K. Tuominen, Phys. Lett. B **497** (2001) 39.
19. P.F. Kolb, J. Sollfrank and U. Heinz, Phys. Lett. B **459** (1999) 667; P.F. Kolb, J. Sollfrank, P.V. Ruuskanen, and U. Heinz, Nucl. Phys. **A661** (1999) 349.
20. B.B. Back *et al.* (PHOBOS Collaboration), Phys. Rev. Lett. **85** (2000) 3100.
21. P. Huovinen, P.F. Kolb, U. Heinz, P.V. Ruuskanen, and S.A. Voloshin, Phys. Lett. B **503** (2001) 58.
22. The transparencies and plots of this and the other talks can be found at the URL ‘<http://theo08.nsl.msu.edu/winterworkshop/proceedings/toc.htm>’
23. D. Kharzeev and M. Nardi, nucl-th/ 0012025.